engineering proceedings

MDPI

Proceeding Paper

First-Principles Calculation Analysis on Electronic Structures and Molecular Dynamics of Gadolinium-Doped $FAPbI_3$ †

Atsushi Suzuki * and Takeo Oku

Department of Materials Chemistry, The University of Shiga Prefecture, 2500 Hassaka, Hikone, Shiga 522-8533, Japan; oku@mat.usp.ac.jp

* Correspondence: suzuki@mat.usp.ac.jp; Tel.: +81-749-28-8369

† Presented at the 4th International Electronic Conference on Applied Sciences, 27 October–10 November 2023; Available online: https://asec2023.sciforum.net/.

Abstract: First-principle calculation analysis on electronic structures and molecular dynamics was performed to investigate addition of gadolinium ion into the formamidinium lead iodine ($FAPbI_3$) perovskite crystal for use in application of photovoltaic devices with stability of performance. The band dispersion, density of state, enthalpy, and kinetic energy were expected during the relaxation process. The Gd-doped $FAPbI_3$ perovskite crystal had effective mass ratio to be 0.02 in narrow band dispersion consisting of 5d and 4f orbital of gadolinium ion, 6p orbital of lead ion, and 5p orbital of iodine ion, supporting the charge transfer and carrier diffusion related to carrier mobility as photovoltaic parameter. The molecular dynamics of the Gd-doped perovskite crystal indicate dynamic stability while suppressing decomposition with separation between nitrogen and hydrogen ions on FA in the crystal. The first-principle calculation expect that the Gd-doped $FAPbI_3$ perovskite crystal have advantage to apply the perovskite solar cell with stability of the photovoltaic performance.

Keywords: electronic structure; molecular dynamics; gadolinium; perovskite; photovoltaic property

1. Introduction

Metal halide perovskite crystal have been fabricated and characterized for development of industrial materials on photovoltaic devices. Material design and performance prediction of perovskite crystal have been performed for development of perovskite solar cell with optimizing the photovoltaic performance [1–10]. Electronic structure, band distribution with effective mass ratio and band gap were expected by first-principle calculation [11–14]. The photovoltaic properties were based on crystal structure, morphology, and 2/3-dimension interfacial formation [15]. The interface passivation on the crystal grain in the perovskite layer suppressed the carrier trap near defect and pinhole in the perovskite layer, extending carrier life and diffusion related to mobility as the photovoltaic parameters [16–24].

Lanthanide doped perovskite crystal have been used for development of the electronic devices such as wavelength convertor, ultra-visible-near-infrared absorption and luminescence [25–30]. The lanthanide ion at multivalent state caused shuttle redox reaction involving in the redox of lead and halogen ion to regenerate the crystal degradation. For example, slight addition of europium, gadolinium (Gd^{2+}), samarium and cerium ions suppressed the decomposition with shuttle redox reaction, reforming the perovskite crystal to achieve a long-term stability of the performance [31,32]. The photovoltaic properties were also related to the band structure with effective mass of hole and electron. Molecular dynamics have been applied for expecting the reaction mechanism, crystal nucleation, formation, decomposition, and energies together with ion diffusion [33–40]. The purpose of this study is to focus on characterization of band structure and molecular dynamics of

Citation: Suzuki, A.; Oku, T. First-Principles Calculation Analysis on Electronic Structures and Molecular Dynamics of Gadolinium-Doped $FAPbI_3$. *Eng. Proc.* **2023**, *52*, x. https://doi.org/10.3390/xxxxx

Academic Editor(s): Name

Published: date

formamidinium lead iodide ($CH(NH_2)_2PbI_3$: $FAPbI_3$) perovskite crystal doped with Gd^{2+} ion for improving the photovoltaic performance and stability.

2. Calculation

The Gd^{2+}-doped $FAPbI_3$ perovskite crystal was assembled with supercells (2 × 2 × 2) based on the $FAPbI_3$ crystals as a cubic crystal phase (cubic $Pm\bar{3}m$) with experimental lattice constants ($FAPbI_3$: a = 6.3621 Å) [32,33,41–43]. Partial substitution of Gd^{2+} ions for Pb^{2+} cation ion was introduced at center of cubic structure. The ab initio quantum calculations were performed by using the Vanderbilt ultrasoft pseudo-potentials, scalar relativistic generalized gradient approximations, and density functional theory (DFT) (Quantum Espresso, v.5.2.1, Quantum Espresso Foundation, UK). The band structures, effective mass ratio of electron and hole to free electron (m_e^*/m_e and m_h^*/m_e), band gap (E_g) and density of state (DOS) near valence (VB) and conduction band (CB) states were expected.

Car–Parrinello molecular dynamics (CPMD) simulations have been performed with Quantum Espresso. Plane-wave basis set cutoffs for the smooth part of the wave functions and the augmented density were 80 and 320 Ry, respectively. The CPMD simulations were performed during an integration time step of 150 for a total simulation time of 0.018 psec. The enthalpy, kinetic energy and molecular dynamics were followed during the relaxation process near 300 K.

3. Results and Discussion

The first-principle calculation analysis was performed to investigate addition of Gd^{2+} ion into the perovskite crystal on the electron density distribution, band dispersion and DOS. The electron density distribution of the Gd-doped $FAPbI_3$ perovskite crystal is shown in Figure 1a. The partially occupied 6s, 6p, and 5d orbital and fully occupied 4f orbital of Gd^{2+} ion, and partially occupied 5s and 5p orbital of iodine ion as ligand were distributed and overlapped each other, sharing the electron between the Gd^{2+} ion and iodine ion to form the coordination bond. Ligand-metal charge transfer between the Gd^{2+} ion and iodine ion are caused, supporting the carrier generation and diffusion related to carrier mobility as photovoltaic parameter. The band dispersion and DOS are shown in Figure 1b,c. The 5p orbital of iodine ion were widely distributed in the range from −3 eV to −2 eV near VB state, and 6p orbital of lead ion, 5d orbitals and 4f orbital of Gd^{2+} ion were also distributed in the range from 0 eV to 1.5 eV near CB state. Effective mass ratio (m_e^*/m_e and m_h^*/m_e) were calculated to be 0.02 and 0.02 from the band dispersion near VB and CB states. The direct band gap (E_g) at the Γ position as *k*-vector was obtained to be about 1.52 eV, as semi-conductive characteristics. The Gd^{2+}-doped $FAPbI_3$ crystal had the narrow band dispersion with the same order of effective mass ratio, as similar to those of the $FAPbI_3$ crystal. The photovoltaic performance related to short circuit current density based on the carrier mobility will be maintained. The formation energies of the Gd^{2+}-doped crystal and $FAPbI_3$ crystal were obtained to be −4662 eV $cell^{-1}$ and −3745 eV $cell^{-1}$, which indicates stability of the Gd^{2+}-doped $FAPbI_3$ crystal.

Enthalpy and kinetic energy of the Gd^{2+}-doped $FAPbI_3$ and $FAPbI_3$ crystal was calculated for expecting the crystal formation, dynamic stability and kinetics of reaction mechanism such as decomposition. The dynamic behaviors regarding the enthalpy and kinetic energy during the relaxation time are shown in Figure 2a. In both cases, similar behavior of the kinetic energies was qualitatively demonstrated. Addition of Gd^{2+} ion into the perovskite crystal caused a gradual decreasing behavior of the enthalpy during the relaxation time. The energy fluctuations were based on the crystal stability with slight distortion of the coordination structure. The kinetic energies behavior of the Gd^{2+}-doped $FAPbI_3$ crystal as similar to those of the $FAPbI_3$ crystal indicate dynamic stability as reaching equilibrium at the final stage. The kinetic energy behavior was derived from the dynamic stability related with degree of distortion of the coordination structure with variation in the position of FA, Gd^{2+} ion and iodine ion as ligand. The structural distortions and molecular

dynamics would be suppressed by the addition of Gd^{2+} ion. For making clear the dynamic behavior, the structural distortion of FA in the Gd^{2+}-doped $FAPbI_3$ crystal and $FAPbI_3$ crystal was characterized by molecular dynamics calculation.

Distance of nitrogen (N) and hydrogen (H) atom in FA of the Gd^{2+}-doped $FAPbI_3$ crystal and $FAPbI_3$ crystal were considered as shown in Figure 2b. In the case of the $FAPbI_3$ crystal, the distance of N-H band in FA was drastically increased, as separation between N-H bands in FA at time of 0.0169 psec. The atomic position of Pb^{2+} ion located in the center of the $FAPbI_3$ crystal was shifted, shrinking the coordination structure in the perovskite crystal as the decomposition. The distortion of crystal structures was induced with a reduction in the thermal energy. In the case of the Gd^{2+}-doped $FAPbI_3$ crystal, the distance between N and H atom in FA was slightly decreased, as dynamic stability of FA. The atomic position of Pb^{2+} ion located in the center of the coordination structure was maintained at final stage. Addition of Gd^{2+} ion into the crystal maintained stabilization, while suppressing the crystal distortions and the separation between N-H bands in FA as decomposition. The calculation prediction indicates that the Gd^{2+}-doped $FAPbI_3$ perovskite crystal have advantage to apply the photovoltaic devices with the stability of performance.

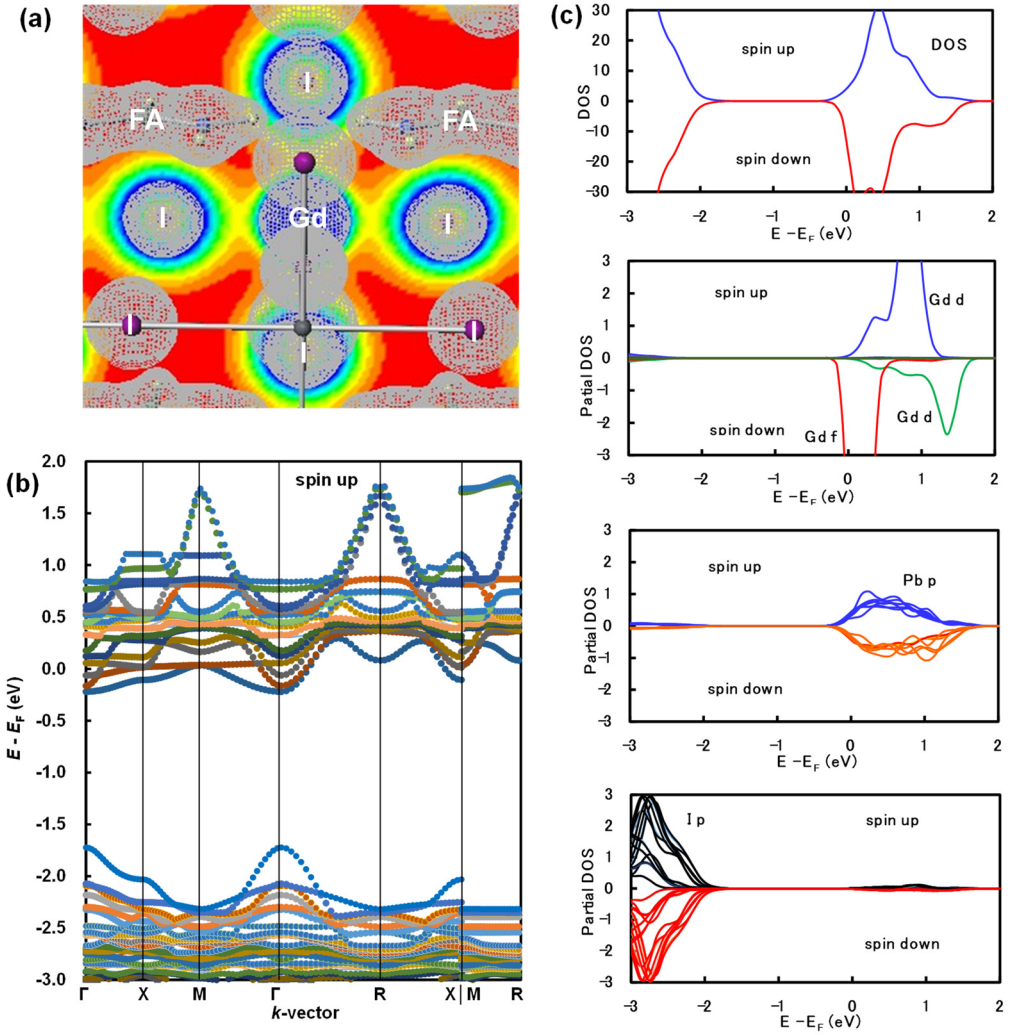

Figure 1. (**a**) Electron density distribution (**b**) band dispersion and (**c**) DOS of the Gd-doped $FAPbI_3$ perovskite crystal.

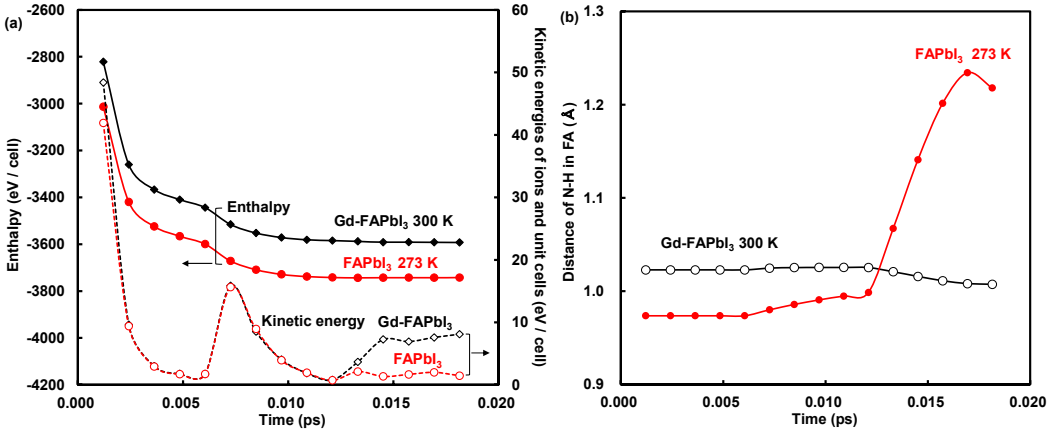

Figure 2. (**a**) Enthalpy, kinetic energy, and (**b**) distance of N-H in FA of (**b**) Gd^{2+}-doped $FAPbI_3$ crystal.

4. Conclusions

The first-principles calculation expected the band dispersion, DOS, electron density distribution, enthalpy, kinetic energy, and molecular dynamics of the Gd^{2+}-doped $FAPbI_3$ crystal, as compared with those of the $FAPbI_3$ crystal. The Gd^{2+}-doped $FAPbI_3$ crystal had the effective mass ratio to be 0.02 in the narrow band dispersion consisting of 5d orbital of Gd^{2+} ion, 6p orbital of Pb^{2+} ion, and 5p orbital of I^- ion as ligand, causing the metal-ligand charge transfer, carrier generation and diffusion related to the mobility as the photovoltaic parameter. The molecular dynamics indicates more dynamic stability and crystal formation for the Gd^{2+}-doped $FAPbI_3$ crystal rather than the $FAPbI_3$ crystal while suppressing the decomposition with the separation of N-H band on FA. The first-principles calculation analysis expects that the Gd^{2+}-$FAPbI_3$ doped crystal have advantage to apply the perovskite solar cell with stability of the photovoltaic performance.

Author Contributions: Conceptualization, A.S.; methodology, A.S.; software, A.S.; validation, A.S.; formal analysis, A.S.; investigation, A.S.; resources, A.S.; data curation, A.S.; writing—original draft preparation, A.S.; writing—review and editing, A.S. and T.O.; visualization, A.S.; supervision, T.O.; project administration, A.S. and T.O.; funding acquisition, A.S. and T.O. All authors have read and agreed to the published version of the manuscript.

Funding: This research was funded by JSPS KAKENHI, grant number 21K05261.

Institutional Review Board Statement: Not applicable.

Informed Consent Statement: Not applicable.

Data Availability Statement: All data generated and analyzed during this study are included in this published article.

Conflicts of Interest: The authors declare no conflict of interest.

References

1. Li, C.; Wang, X.; Bi, E. ; Jiang, F.; Park, S.M.; Li, Y.; Chen, L. ; Wang, Z.; Zeng, L.; Chen, H.; et al. Rational design of Lewis base molecules for stable and efficient inverted perovskite solar cells. *Science* **2023**, *379*, 690–694. https://doi.org/10.1126/science.ade3970.
2. Li, Z.; Wang, X.; Wang, Z.; Shao, Z.; Hao, L.; Rao, Y.; Chen, C.; Liu, D.; Zhao, Q.; Sun, X.; et al. Ammonia for post-healing of formamidinium-based Perovskite films. *Nat. Comm.* **2022**, *13*, 4417. https://doi.org/10.1038/s41467-022-32047-z.
3. Wu, Y.; Wang, Q.; Chen, Y.; Qiu, W.; Peng, Q. Stable perovskite solar cells with 25.17% efficiency enabled by improving crystallization and passivating defects synergistically. *Energy Environ. Sci.* **2022**, *15*, 4700–4709. https://doi.org/10.1039/D2EE02277J.
4. Wu, X.; Zhang, D.; Wang, X.; Jiang, X.; Liu, B.; Li, B.; Li, Z.; Gao, D.; Zhang, C.; Wang, Y.; et al. Eco-friendly perovskite solar cells: From materials design to device processing and recycling. *EcoMat* **2023**, *5*, e12352. https://doi.org/10.1002/eom2.12352.

5. Ono, I.; Oku, T.; Suzuki, A.; Asakawa, Y.; Terada, S.; Okita, M.; Fukunishi, S.; Tachikawa, T. Fabrication and characterization of $CH_3NH_3PbI_3$ solar cells with added guanidinium and inserted with decaphenylpentasilane. *Jpn. J. Appl. Phys.* **2022**, *61*, SB1024. https://doi.org/10.35848/1347-4065/ac2661.
6. Okumura, R.; Oku, T.; Suzuki, A.; Okita, M.; Fukunishi, S.; Tachikawa, T.; Hasegawa, T. Effects of adding alkali metals and organic cations to Cu-based perovskite solar cells. *Appl. Sci.* **2022**, *12*, 1710. https://doi.org/10.3390/app12031710.
7. Enomoto, A.; Suzuki, A.; Oku, T.; Okita, M.; Fukunishi, S.; Tachikawa, T.; Hasegawa, T. Effects of Cu, K and guanidinium addition to $CH_3NH_3PbI_3$ perovskite solar cells. *J. Electron. Mater.* **2022**, *51*, 4317–4328. https://doi.org/10.1007/s11664-022-09688-3.
8. Asakawa, Y.; Oku, T.; Kido, M.; Suzuki, A.; Okumura, R.; Okita, M.; Fukunishi, S.; Tachikawa, T.; Hasegawa, T. Fabrication and characterization of $SnCl_2$- and CuBr-added perovskite photovoltaic devices. *Technologies* **2022**, *10*, 112. https://doi.org/10.3390/technologies10060112.
9. Terada, S.; Oku, T.; Suzuki, A.; Okita, M.; Fukunishi, S.; Tachikawa, T.; Hasegawa, T. Ethylammonium bromide- and potassium-added $CH_3NH_3PbI_3$ perovskite solar cells. *Photonics* **2022**, *9*, 791. https://doi.org/10.3390/photonics9110791.
10. Enomoto, A.; Suzuki, A.; Oku, T.; Fukunishi, S.; Tachikawa, T.; Hasegawa, T. First-principles calculations and device characterizations of formamidinium-cesium lead triiodide perovskite crystals stabilized by germanium or copper. *Jpn. J. Appl. Phys.* **2023**, *62*, SK1015. https://doi.org/10.35848/1347-4065/acc6d8.
11. Hossain, M.K.; Toki, G.F.I.; Kuddus, A.; Rubel, M.H.K.; Hossain, M.M.; Bencherif, H.; Rahman, M.F.; Islam, M.R.; Mushtaq, M. An extensive study on multiple ETL and HTL layers to design and simulation of high-performance lead-free $CsSnCl_3$-based perovskite solar cells. *Sci. Rep.* **2023**, *13*, 2521. https://doi.org/10.1038/s41598-023-28506-2.
12. Hossain, M.K.; Mohammed, M.K.A.; Pandey, R.; Arnab, A.A.; Rubel, M.H.K.; Hossain, K.M.; Ali, M.H.; Rahman, M.F.; Bencherif, H.; Madan, J.; et al. Numerical analysis in DFT and SCAPS-1D on the influence of different charge transport layers of $CsPbBr_3$ perovskite solar cells. *Energy Fuels* **2023**, *37*, 6078. https://doi.org/10.1021/acs.energyfuels.3c00035.
13. Hossain, M.K.; Toki, G.F.I.; Samajdar, D.P.; Mushtaq, M.; Rubel, M.H.K.; Pandey, R.; Madan, J.; Mohammed, M.K.A.; Islam, M.R.; Rahman, M.F.; et al. Deep insights into the coupled optoelectronic and photovoltaic analysis of lead-free $CsSnI_3$ perovskite-based solar cell using DFT calculations and SCAPS-1D simulations. *ACS Omega* **2023**, *8*, 22466-22485. https://doi.org/10.1021/acsomega.3c00306.
14. Diao, X.; Diao, Y.; Tang, Y.; Zhao, G.; Gu, Q.; Xie, Y.; Shi, Y.; Zhu, P.; Zhang, L. High-throughput screening of stable and efficient double inorganic halide perovskite materials by DFT. *Sci. Rep.* **2022**, *12*, 12633. https://doi.org/10.1038/s41598-022-16221-3.
15. Ma, C.; Eickemeyer, F.T.; Lee, S.H.; Kang, D.H.; Kwon, S.J.; Grätzel, M.; Park, N.G. Unveiling facet-dependent degradation and facetengineering for stable perovskite solar cells. *Science* **2023**, *379*, 173–178. https://doi.org/10.1126/science.adf3349.
16. Chin, X.Y.; Turkay, D.; Steele, J.A.; Tabean, S.; Eswara, S.; Mensi, M.; Fiala, P.; Wolff, C.M.; Paracchino, A.; Artuk, K.; et al. Interface passivation for 31.25%-efficient perovskite/silicon tandem solar cells. *Science* **2023**, *381*, 59–63. https://doi.org/10.1126/science.adg0091.
17. Xia, J.; Liang, C.; Gu, H.; Mei, S.; Li, S.; Zhang, N.; Chen, S.; Cai, Y.; Xing, G. Surface passivation toward efficient and stable perovskite solar cells. *Energy Environ. Mater.* **2023**, *6*, e12296. https://doi.org/10.1002/eem2.12296.
18. Ren, J.; Liu, T.; He, B.; Wu, G.; Gu, H.; Wang, B.: Li, J.; Mao, Y.; Chen, S.; Xing, G. Passivating defects at the bottom interface of perovskite by ethylammonium to improve the performance of perovskite solar cells. *Small* **2022**, *18*, 2203536. https://doi.org/10.1002/smll.202203536.
19. Li, C.; Wang, X.; Bi, E.; Jiang, F.; Park, S.M.; Li, Y.; Chen, L.; Wang, Z.; Zeng, L.; Chen, H.; et al. Rational design of Lewis base molecules for stable and efficient inverted perovskite solar cells. *Science* **2023**, *379*, 690–694. https://doi.org/10.1126/science.ade3970.
20. Azmi, R.; Ugur, E.; Seitkhan, A.; Aljamaan, F.; Subbiah, A.S.; Liu, J.; Harrison, G.T.; Nugraha, M.I.; Eswaran, M.K.; Babics, M.; et al. Damp heat–stable perovskite solar cells with tailored-dimensionality 2D/3D heterojunctions. *Science* **2022**, *376*, 73–77. https://doi.org/10.1126/science.abm5784.
21. Fu, Y.; Li, Y.; Xing, G.; Cao, D. Surface passivation of perovskite with organic hole transport materials for highly efficient and stable perovskite solar cells. *Mater. Mater. Today Adv.* **2022**, *16*, 100300. https://doi.org/10.1016/j.mtadv.2022.100300.
22. Lin, R.; Xu, J.; Wei, M.; Wang, Y.; Qin, Z.; Liu, Z.; Wu, J.; Xiao, K.; Chen, B.; Park, S.M.; et al. All-perovskite tandem solar cells with improved grain surface passivation. *Nature* **2022**, *603*, 73–78. https://doi.org/10.1038/s41586-021-04372-8.
23. Suzuki, A.; Hasegawa, R.; Funayama, K.; Oku, T.; Okita, M.; Fukunishi, S.; Tachikawa, T.; Hasegawa, T. Additive effects of $CuPcX_4$-TCNQ on $CH_3NH_3PbI_3$ perovskite solar cells. *J. Mater. Sci. Mater. Electron.* **2023**, *34*, 588. https://doi.org/10.1007/s10854-023-10001-z.
24. Ogawa, C.; Suzuki, A.; Oku, T.; Fukunishi, S.; Tachikawa, T.; Hasegawa, T. Metallophtalocyanine used interface engineering for improving long-term stability of methylammonium lead triiodide perovskite. *Phys. Status Solidi A* **2023**, *220*, 2300038. https://doi.org/10.1002/pssa.202300038.
25. Kachhap, S.; Singh, S.; Singh, A.K.; Singh, S.K. Lanthanide-doped inorganic halide perovskites ($CsPbX_3$): Novel properties and emerging applications. *J. Mater. Chem. C* **2022**, *10*, 3647. https://doi.org/10.1039/D1TC05506B.
26. Samanta, T.; Mukurala, N.; Viswanath, N.S.M.; Han, J.H.; Cho, H.B.; Min, J.W.; Jung, S.W.; Park, Y.; Chung, W.J.; Im, W.B. Recent progress in lanthanide-based metal halide perovskites: Synthesis, properties, and applications. *Opt. Mater. X* **2023**, *18*, 100238. https://doi.org/10.1016/j.omx.2023.100238.

27. Wang, L.; Zhou, H.; Hu, J.; Huang, B.; Sun, M.; Dong, B.; Zheng, G.; Huang, Y.; Chen, Y.; Li, L.; et al. A Eu^{3+}-Eu^{2+} ion redox shuttle imparts operational durability to Pb-I perovskite solar cells. *Science* **2019**, *363*, 265–270. https://doi.org/10.1126/science.aau5701.
28. Mir, W.J.; Sheikh, T.; Arfin, H.; Xia, Z.; Nag, A. Lanthanide doping in metal halide perovskite nanocrystals: Spectral shifting, quantum cutting and optoelectronic applications. *NPG Asia Mater.* **2020**, *12*, 9. https://doi.org/10.1038/s41427-019-0192-0.
29. Lee, M.; Lee, D.H.D.; Hong, S.V.; Woo, H.Y.; Chae, J.-Y.; Lee, D.W.; Han, M.J.; Paik, T. Highly luminescent and multifunctional zero-dimensional cesium lanthanide chloride (Cs_3LnCl_6) colloidal nanocrystals. *Adv. Opt. Mater.* **2022**, *10*, 2102727. https://doi.org/10.1002/adom.202102727.
30. Zhang, L.; Yuan, M. Lanthanide doped lead-free double perovskites as the promising next generation ultra-broadband light sources. *Light Sci. Appl.* **2022**, *11*, 99. https://doi.org/10.1038/s41377-022-00782-z.
31. Yang, Y.; Wu, J.; Wang, X.; Guo, Q.; Liu, X.; Sun, W.; Wei, Y.; Huang, Y.; Lan, Z.; Huang, M.; et al. Suppressing vacancy defects and grain boundaries via ostwald ripening for high-performance and stable perovskite solar cells. *Adv. Mater.* **2020**, *32*, 1904347. https://doi.org/10.1002/adma.201904347.
32. Suzuki, A.; Kishimoto, K.; Oku, T.; Okita, M.; Fukunishi, S.; Tachikawa, T. Additive effect of lanthanide compounds into perovskite layer on photovoltaic properties and electronic structures. *Synth. Met.* **2022**, *287*, 117092. https://doi.org/10.1016/j.synthmet.2022.117092.
33. Suzuki, A.; Oku, T. Electronic structures and molecular dynamics of gadolinium-doped $FAPbI_3$ perovskite crystals. *Jpn. J. Appl. Phys.* **2023**, *62*, SK1006. https://10.35848/1347-4065/acbec0.
34. Fransson, E.; Rosander, P.; Eriksson, F.; Rahm, J.M.; Tadano. T.; Erhart, P. Limits of the phonon quasi-particle picture at the cubic-to-tetragonal phase transition in halide perovskites. *Commun. Phys.* **2023**, *6*, 173. https://doi.org/10.1038/s42005-023-01297-8.
35. Kaiser, W.; Mosconi, E.; Alothman, A.A.; Meggiolaro, D.; Gagliardi, A.; Angelis, F.D. Halide-driven formation of lead halide perovskites: Insight from ab initio molecular dynamics simulations. *Mater. Adv.* **2021**, *2*, 3915–3926. https://doi.org/10.1039/d1ma00371b.
36. Ning, J.; Zheng, L.; Lei, W.; Wang, S.; Xi, J.; Yang, J. Temperature-dependence of the band gap in the all-inorganic perovskite $CsPbI_3$ from room to high temperatures. *Phys. Chem. Chem. Phys.* **2022**, *24*, 16003–16010. https://doi.org/10.1039/D2CP00940D.
37. Kaiser, W.; Ricciarelli, D.; Mosconi, E.; Alothman, A.A.; Ambrosio, F.; Angelis, F.D. Stability of tin-versus lead-halide perovskites: Ab initio molecular dynamics simulations of perovskite/water interfaces. *J. Phys. Chem. Lett.* **2022**, *13*, 2321–2329. https://doi.org/10.1021/acs.jpclett.2c00273.
38. Tseng, M.-L.; Adesiyan, A.; Gassoumi, A.; Gorji, N.E. A molecular dynamics study of water confined in between two graphene sheets under compression. *J. Nanopart. Res.* **2023**, *25*, 51. https://doi.org/10.1007/s11051-023-05698-2.
39. Arora, N.; Greco, A.; Meloni, S.; Hinderhofer, A.; Mattoni, A.; Rothlisberger, U.; Hagenlocher, J.; Caddeo, C.; Zakeeruddin, S.M.; Schreiber, F.; et al. Kinetics and energetics of metal halide perovskite conversion reactions at the nanoscale. *Commun. Mater.* **2022**, *3*, 22. https://doi.org/10.1038/s43246-022-00239-1.
40. Shi, R.; Guo, M.; Long, R. Improved defect tolerance and charge carrier lifetime in tin–lead mixed perovskites: Ab Initio quantum dynamics, *J. Phys. Chem. Lett.* **2023**, *14*, 499–507. https://doi.org/10.1021/acs.jpclett.2c03649.
41. Weller, M.T.; Weber, O.J.; Frost, J.M.; Walsh, A. Cubic perovskite structure of black formamidinium lead iodide, α-$[HC(NH_2)_2]PbI_3$, at 298 K. *J. Phys. Chem. Lett.* **2015**, *6*, 3209–3212. https://doi.org/10.1021/acs.jpclett.5b01432.
42. Mashiyama, H.; Kurihara, Y.; Azetsu, T. Disordered cubic perovskite structure of $CH_3NH_3PbX_3$ (X = Cl, Br,I). *J. Korean Phys. Soc.* **1998**, *32*, S156–S158.
43. Oku, T. Crystal structures of perovskite halide compounds used for solar cells. *Rev. Adv. Mater. Sci.* **2020**, *59*, 264–305. https://doi.org/10.1515/rams-2020-0015.